Electronic Supplementary Material (ESI) for Journal of Materials Chemistry C.

Supporting Information

Robust and flexible composite aerogel films with porous multilayered structures toward broadband electromagnetic wave absorption

Zhihui Li[a,b], Chenhui Xu[a], Jiajia Zheng[a], Tianyi Hang[a], Yiming Chen[a,*], Hongjun Lin[c], Xiping Li[a], Zhiyi Wu[b,*]

[a] *Key Laboratory of Urban Rail Transit Intelligent Operation and Maintenance Technology & Equipment of Zhejiang Province, College of Engineering, Zhejiang Normal University, Jinhua 321004, China.*

[b] *Beijing Institute of Nanoenergy and Nanosystems, Chinese Academy of Sciences, Beijing 100083, China.*

[c] *College of Geography and Environmental Sciences, Zhejiang Normal University, Jinhua 321004, China.*

**Emails: yiming.chen@zjnu.edu.cn (Y. Chen); wuzhiyi@binn.cas.cn (Z. Wu)*

Supporting Information Corresponding Formulas

S1. Electromagnetic parameters measurement

The electromagnetic parameters including complex permittivity and complex permeability of the composite aerogel films were measured within the frequency range of 2-18 GHz. The *RL-f* curve is calculated using the measured electromagnetic parameters based on the following equations:

$$RL(dB) = 20\log\left|\frac{Z_{in} - Z_0}{Z_{in} + Z_0}\right| \qquad \text{(Eq. S1)}$$

$$\frac{Z_{in}}{Z_0} = \sqrt{\frac{\mu_r}{\varepsilon_r}}\tanh\left[j\frac{2\pi fd}{c}\sqrt{\mu_r\varepsilon_r}\right] \qquad \text{(Eq. S2)}$$

where Z_{in} represents the input impedance of the absorber, Z_0 is the impedance of free space,[1] ε_r is the relative complex permittivity, μ_r is the relative complex permeability, f is the frequency, d is the sample thickness, and c is the speed of light.

S2. Debye relaxation

Dielectric polarization refers to the phenomenon where bound charges migrate along the direction of an applied electric field, resulting in electron displacement or alignment of dipoles. In high-frequency electromagnetic fields, when the motion of electrons or the reorientation of dipoles cannot keep up with the changes under the alternating electric field, a lagging effect of electron or dipole polarization relaxation occurs. The Cole-Cole semicircle equation based on the Debye relaxation theory can effectively contribute to understanding the relaxation processes that occur under the influence of alternating electromagnetic fields based on the following equations:

$$\varepsilon' = \varepsilon_\infty + \frac{\varepsilon_s - \varepsilon_\infty}{1 + \omega^2\tau^2} \qquad \text{(Eq. S3)}$$

$$\varepsilon'' = \frac{\varepsilon_s - \varepsilon_\infty}{1+\omega^2\tau^2}\omega\tau + \frac{\sigma}{\omega\varepsilon_0} \quad \text{(Eq. S4)}$$

where ε_∞ represents the relative dielectric constant at high-frequency limit, ε_s denotes the static dielectric constant, ω refers to the angular frequency, τ is the polarization relaxation time, and σ is the conductivity. From Eq. S3 and Eq. S4, we can obtain the relationship between ε' and ε'':[2]

$$\left(\varepsilon' - \frac{\varepsilon_s + \varepsilon_\infty}{2}\right)^2 + (\varepsilon'')^2 = \left(\frac{\varepsilon_s - \varepsilon_\infty}{2}\right)^2 \quad \text{(Eq. S5)}$$

It should be noted that each Cole-Cole semicircle corresponds to a Debye relaxation process.

S3. Quarter-wavelength resonance formula

$$f_m = \frac{(2N-1)c}{4 t_m n} \quad \text{(Eq. S6)}$$

where f_m is the resonance peak frequency and t_m is the resonance thickness of the sample. While n is the real part of square root of the product of complex permittivity and permeability, and N is a positive integer.

S4. Impedance matching

The attenuation constant (α), which mainly determines the attenuation capability of the incident EMWs, can be expressed based on the following equation:

$$\alpha = \frac{\sqrt{2}\pi f}{c}\sqrt{(\mu''\varepsilon'' - \mu'\varepsilon') + \sqrt{(\mu''\varepsilon'' - \mu'\varepsilon')^2 + (\mu'\varepsilon'' + \mu''\varepsilon')^2}} \quad \text{(Eq. S7)}$$

To achieve high-performance EMW absorption, it is quite important that the incident EMWs should enter the absorber as much as possible. Therefore, a good impedance matching at the air-material interface is extremely necessary and critical. According to Eq. S1 and Eq. S2, the best impedance matching can be obtained when the Z ($|Z_{in}/Z_0|$) value is close or equal to 1 ($Z_{in} = Z_0$), and the RL will reach its optimal value.[3]

Supporting Information Corresponding Figures and Table

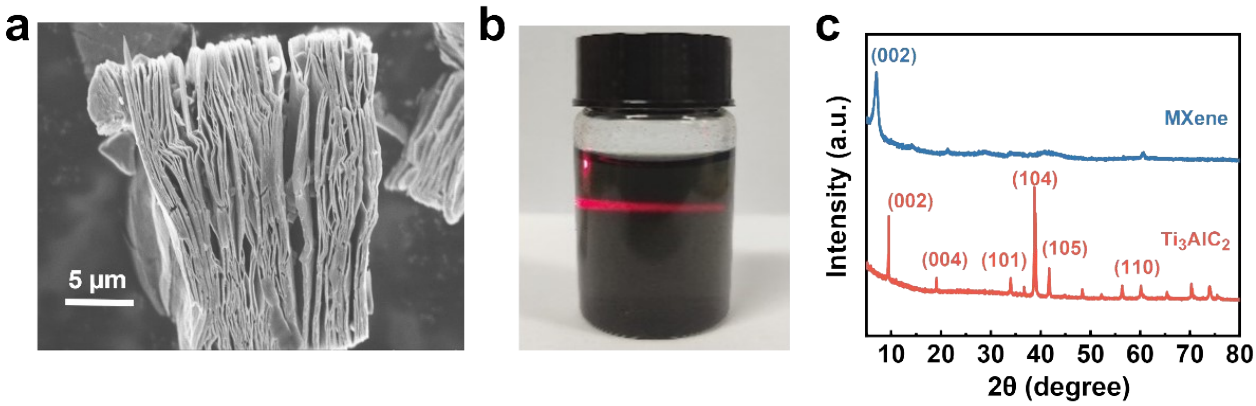

Fig. S1. (a) SEM image of the multilayered $Ti_3C_2T_x$. (b) Digital imaging of the Tyndall effect produced by $Ti_3C_2T_x$ suspensions. (c) XRD patterns of MAX phase and $Ti_3C_2T_x$.

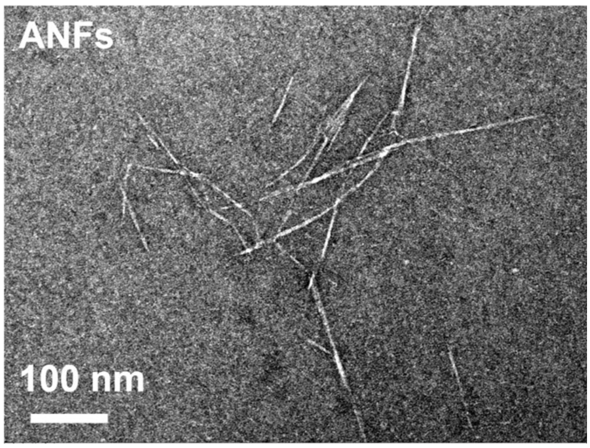

Fig. S2. TEM image of ANFs.

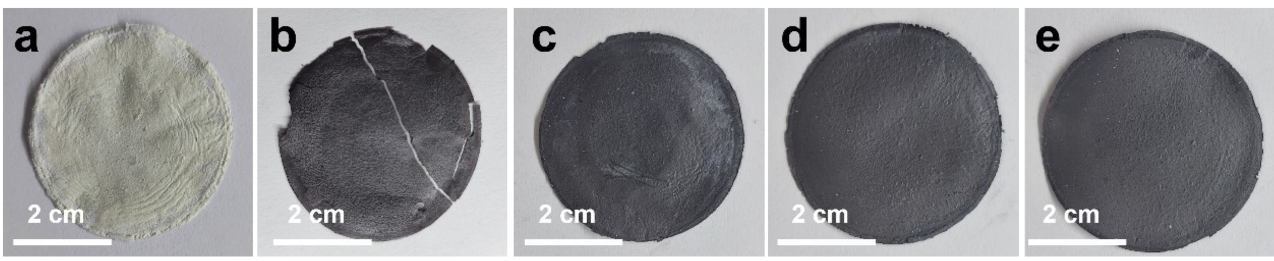

Fig. S3. Digital images of the (a) pure ANF film, (b) pure MXene film, (c) AM, (d) AMN-1, and (e) AMN-3.

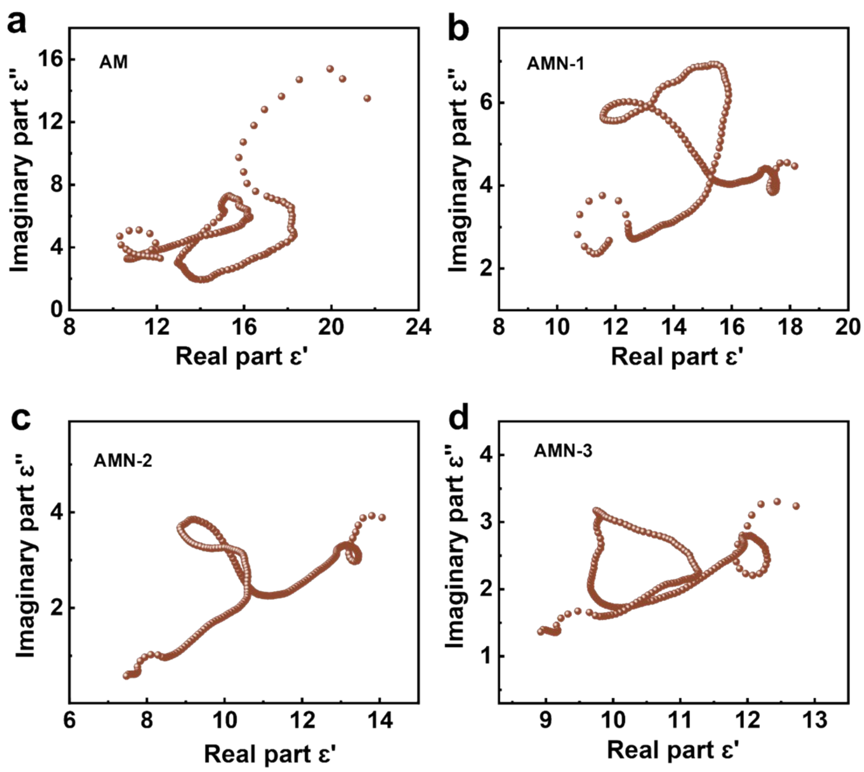

Fig. S4. Cole-Cole curves of (a) AM, (b) AMN-1, (c) AMN-2, and (d) AMN-3.

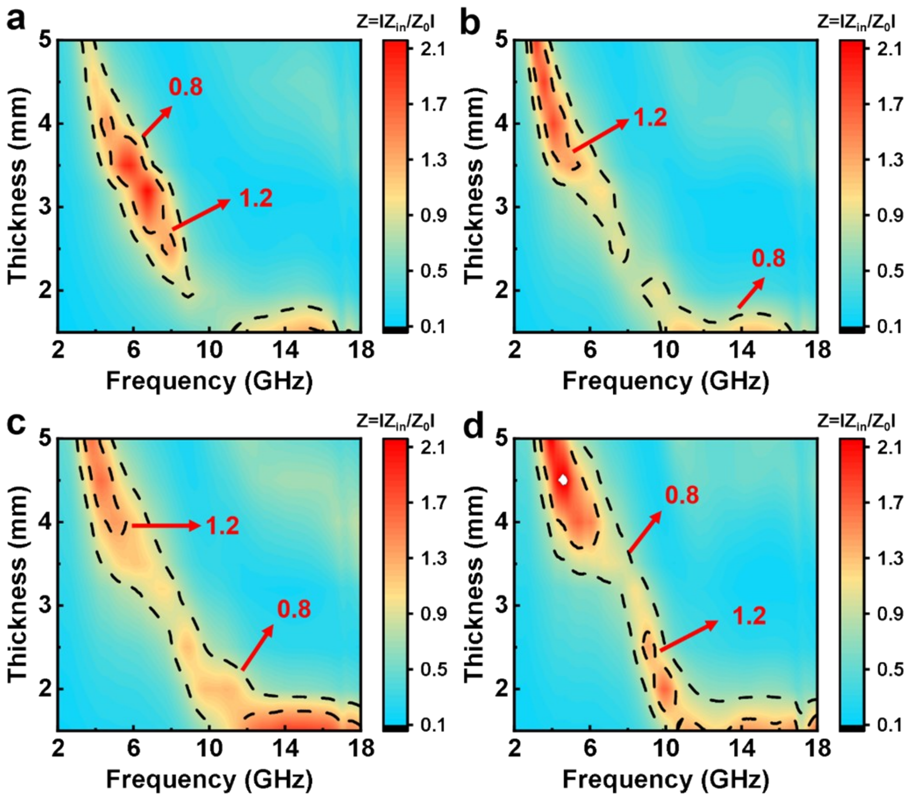

Fig. S5. The values of $Z = |Z_{in}/Z_0|$ of (a) AM, (b) AMN-1, (c) AMN-2, and (d) AMN-3.

Table S1. Comparison of EMW absorption properties of the AMN aerogel film with other related MXene-based composites.

Samples	*RL* (dB)	*EAB* (GHz)	Matching thickness (mm)	Ref.
$Fe_3O_4@Ti_3C_2T_x$	-57.2	1.4	4.2	[4]
MXene/Ni	-49.9	2.1	1.75	[5]
MXene/Ni	-31.9	2.3	1.0	[6]
MXene-CoC	-46.48	3.0	1.02	[7]
$Ti_3C_2T_x/Fe_3O_4$	-50.18	3.2	1.3	[8]
Ni@MXene	-52.6	3.7	3.0	[9]
MXene-CNTs/Ni	-56.4	3.95	2.4	[10]
$Co/ZnO@CNTs/Ti_3C_2T_x$	-46.0	4.0	1.9	[11]
MXene/RGO	-44.3	4.84	1.5	[12]
MXene-rGO/CoNi	-54.1	4.9	2.01	[13]
MXene/Ni	-50.5	5.28	3.5	[14]
MXene/RGO	-31.2	5.4	2.05	[15]
ANF/MXene/Ni	-48.6	5.8	1.5	This work

References

1. C. Wang, V. Murugadoss, J. Kong, Z. He, X. Mai, Q. Shao, Y. Chen, L. Guo, C. Liu, S. Angaiahand Z. Guo, *Carbon*, 2018, **140**, 696-733.
2. N. Yang, Z.-X. Luo, G.-R. Zhu, S.-C. Chen, X.-L. Wang, G. Wu and Y.-Z. Wang, *ACS Appl. Mater. Interfaces*, 2019, **11**, 35987-35998.
3. M. Green and X. Chen, *J. Materiomics*, 2019, **5**, 503-541.
4. X. Zhang, H. Wang, R. Hu, C. Huang, W. Zhong, L. Pan, Y. Feng, T. Qiu, C. Zhang and J. Yang, *Appl. Surf. Sci.*, 2019, **484**, 383-391.
5. L. Liang, G. Han, Y. Li, B. Zhao, B. Zhou, Y. Feng, J. Ma, Y. Wang, R. Zhang and C. Liu, *ACS Appl. Mater. Interfaces*, 2019, **11**, 25399-25409.
6. F. Pan, Y. Rao, D. Batalu, L. Cai, Y. Dong, X. Zhu, Y. Shi, Z. Shi, Y. Liu and W. Lu, *Nanomicro lett.*, 2022, **14**, 140.
7. F. Pan, L. Yu, Z. Xiang, Z. Liu, B. Deng, E. Cui, Z. Shi, X. Li and W. Lu, *Carbon*, 2021, **172**, 506-515.
8. Y. Li, Y. Gao, B. Fan, L. Guan, B. Zhao and R. Zhang, *J. Phys. Chem. C*, 2021, **125**, 19914-19924.
9. L. Liang, R. Yang, G. Han, Y. Feng, B. Zhao, R. Zhang, Y. Wang and C. Liu, *ACS Appl. Mater. Interfaces*, 2020, **12**, 2644-2654.
10. X. Li, W. You, C. Xu, L. Wang, L. Yang, Y. Li and R. Che, *Nanomicro lett.*, 2021, **13**, 157.
11. C. Sun, Q. Li, Z. Jia, G. Wu and P. Yin, *Chem. Eng. J.*, 2023, **454**, 140277.
12. X. Li, D. Xu, D. Zhou, S. Pang, C. Du, M. A. Darwish, T. Zhou and S.-K. Sun, *Carbon*, 2023, **208**, 374-383.

13. X. Li, Z. Wu, W. You, L. Yang and R. Che, *Nanomicro lett.*, 2022, **14**, 73.
14. X. Li, W. You, L. Wang, J. Liu, Z. Wu, K. Pei, Y. Li and R. Che, *ACS Appl. Mater. Interfaces*, 2019, **11**, 44536-44544.
15. L. Wang, H. Liu, X. Lv, G. Cui and G. Gu, *J. Alloys Compd.*, 2020, **828**, 154251.